Zerovalent Irons: Styles of Corrosion and Inorganic Control on Hydrogen Pressure Buildup

ERIC J. REARDON*

Department of Earth Sciences, University of Waterloo, Waterloo, Ontario, Canada N2L 3G1

Apparent corrosion rates have been measured for several commercially available zerovalent irons by monitoring hydrogen evolution in closed cells. Sievert-type rate constants (k_S) were determined to account for hydrogen entering the iron lattice. Thus corrected corrosion rates (R_{corr}) are provided for all irons tested in this study. Because the rate of hydrogen entering the iron lattice increases with $P_{H_2}^{1/2}$, and the rate of hydrogen production from corrosion, far from equilibrium conditions, is independent of P_{H_2}, at some time under closed system conditions the two rates become equal and a steady-state P_{H_2} is attained. A relation describing this condition has been derived: $P_{H_2SS} = [R_{corr}/k_S]^2$ For the granular irons considered in this study, P_{H_2SS} values vary from less than one to eight bars, in contrast to the calculated thermodynamic equilibrium P_{H_2} values for anaerobic corrosion, which range from 138 to 631 bar depending on the assumed product of corrosion. Because groundwater flow at an iron permeable reactive barrier removes hydrogen gas in the dissolved state, P_{H_2SS} values will be less than calculated using the relation above. A method is presented to calculate P_{H_2} values along the flow direction in a PRB, and thus the maximum P_{H_2} value that can possibly develop, assuming no bacterial utilization of the produced hydrogen.

Introduction

Since the early 1990s, granulated zerovalent iron (ZVI) has been used to degrade halogenated hydrocarbons in groundwater, such as trichloromethane (TCM), tetrachloroethene (PCE), and trichloroethene (TCE) (*1*−*5*). Although the exact chemical mechanisms are still a subject of ongoing research (*6*, *7*), the development of anaerobic conditions, the removal or autoreduction of the passive layer, and the establishment of a magnetite or a hydrated magnetite-type layer seems to be a prerequisite for dehalogenation reactions to occur (*8*). Adsorbed hydrogen atoms, such as generated by anaerobic corrosion of the ZVI, may be also involved in the electron exchange required to effect the reductive dehalogenation reactions. Many commercial sources of ZVI currently used to construct permeable reactive barriers (PRBs) have ferric oxides on their particle surfaces. Upon addition of oxygen-free water, these oxides are autoreduced in a few hours to material, which is usually identified by Raman spectroscopy as magnetite (Fe_3O_4) (*7*, *9*). As water penetrates the iron particle surface oxides, anaerobic corrosion begins

$$Fe_{(s)} + 2H_2O_{(l)} \leftrightarrow Fe^{2+} + 2OH^- + H_{2(g)} \qquad (1)$$

where one mole of hydrogen gas and two moles of OH^- are generated for every mole of iron corroded. Equation 1 is an overall reaction and the actual corrosion pathway is more complex, involving single, surface-sorbed hydrogen atoms before they assemble into hydrogen gas (*10*). In the absence of buffering agents, saturation with respect to $Fe(OH)_2$ is very quickly reached (the solubility product K_{sp} is $10^{-14.7}$). Under anaerobic conditions, $Fe(OH)_2$ is unstable and converts to magnetite via the Shikorr reaction at temperatures above approximately 80 °C (*11*):

$$3Fe(OH)_{2(s)} \leftrightarrow Fe_3O_{4(s)} + H_{2(g)} + 2H_2O_{(l)} \qquad (2)$$

$Fe(OH)_2$ converts slowly or not at all at ambient temperatures; however, the conversion can be catalyzed by the presence of ZVI (*12*, *13*). Hydrogen generation associated with reactions 1 and 2 is generally noticeable in batch, and oftentimes column, experiments with ZVI after 1 or 2 days of water contact. Hydrogen evolution is of considerable importance in developing PRB remediation technology. If the rate of hydrogen production exceeds the rate of its removal in the dissolved state, a two-phase flow could develop. The consequence could be the restriction or short-circuiting of groundwater flow through the PRB. On the plus side, the produced hydrogen is a potential fuel source for various microorganisms, whose biochemical activity can potentially carry out other organic degradation reactions at contaminated sites (*14*). Bacterial utilization of hydrogen, however, can lead to biofilm formation in the pore network. This can lead to a decrease in porosity and permeability within the PRB (*15*, *16*).

The purpose of this study is to reveal the diversity of hydrogen evolution behavior for several commercially available irons and to delineate the inorganic controls on both the rates of hydrogen production and the maximum possible pressures attainable in iron/water systems.

Experimental Section

Materials. A record of the ZVI's tested, manufacturer, mesh size, mass of ZVI, water, and void space volume present during the corrosion tests are listed in Table 1.

Information on the presence of soluble material in the tested irons was obtained by reacting 15 g samples with 15 mL of deionized water in 20 mL glass vials. The vials were rotated at 3 rpm on a rotisserie for 60 min, whereupon pH and conductance measurements were taken.

Corrosion Test Apparatus. All corrosion tests were conducted in 150 mL stainless steel cells outfitted with Swagelok fittings to allow void space evacuation, water entry, and pressure measurements. During the test period, the cells were immersed in a constant temperature water bath maintained at 25 ± 0.1 °C. Cell pressures were measured with PX 302 Omega absolute vacuum, 0−15 psi pressure transducers, and readings collected at 1 min intervals using a PC outfitted with a 16-bit data acquisition board manufactured by Strawberry Tree (now produced by IOTECH). Hydrogen uptake by the stainless steel components of the test cell is minimal and does not interfere with determining iron corrosion rates for ZVI samples from the cell's hydrogen pressure increase. For example, the pressure decreases over 30 d in a cell containing 10 mL of water, and no ZVI sample corresponded to < 1 μmol d^{-1} hydrogen uptake at a P_{H_2} of 142 kPa. This compares to hydrogen production rates of 100−3000 μmol d^{-1} measured for the various commercial irons in this study and which are normally carried out at much lower pressures (typically 3−100 kPa).

* Corresponding author phone: (519)888-4567 ext 3234; fax: (519)-746-7484; e-mail: ejreardo@uwaterloo.ca.

10.1021/es050507f CCC: $30.25
Published on Web 08/05/2005

TABLE 1. Information on Iron Samples, Corrosion Test Setup, and Derived Rate Constants (k_S)[a]

iron manufacturer	UW no.	mesh size	mass, g	H_2O, g	V_{Gas}, cm^3	R_{corr}, mmol $kg^{-1}L^{-1}$	k_S, mmol kg^{-1} d^{-1} $kPa^{0.5}$
Master Builders Inc., U.S.A.	NA	+18	267.41	29.94	61.1	0.39	0.013 ± 0.005
Connelly GPM Inc., U.S.A.	223	12−200	217.93	76.5	19.5	0.27	0.015 ± 0.004
Connelly GPM Inc., U.S.A.	NA	12−200	217.93	76.5	19.5	0.15	0.020 ± 0.002
Peerless Metal Powders and Abrasives, U.S.A.	147	8−50	200.65	72.0	19.5	0.14	0.005 ± 0.001
Fisher Scientific (Electrolytic) U.S.A.	NA	−100	14.60	25.0	57.0	79.0	1.5 ± 0.3
Gotthart-Maier Metallpulver, Rheinfelden, Germany	165	12−100	249.72	18.15	63.5	1.15	0.042 ± 0.010
QMP Quebec Metal Powders, Canada	274	12−200	399.07	40.83	30.7	0.162	0.021 ± 0.003
ISPAT Sidbec-Dosco, Quebec, Canada	275	12−200	184.69	69.39	33.6	3.13	0.197 ± 0.012
Fluka Chemie, Switzerland	NA	+18	145.55	48.0	21.2	NA	ND
Fluka Chemie, Switzerland	NA	18−32	74.85	60.0	18.0	NA	ND

[a] ND-not determined; NA-not available or not applicable. UW no. is a cataloguing number system for iron materials maintained by Dr. R. Gillham's research group at the University of Waterloo.

Corrosion Test Procedure. All tests were performed on iron material in an 'as received' condition, i.e., without any washing or other pretreatment. A cell containing a dry iron sample is first evacuated for several hours. Triplicate measurements of the total volume of void space (V_{VS}) are then determined by injection of air or nitrogen gas using a calibrated syringe. Total void space determinations usually agree to within 1 mL. The cell is then weighed, reevacuated, and deionized water added to fully saturate the iron granules. After allowing several minutes for the granules to soak, nitrogen gas is introduced through the top of the cell to displace the drainable water from the bottom. Once water flow is interrupted by nitrogen gas bubbles, the cell is sealed, top and bottom, and reweighed to determine the mass of water present (M_{H_2O}). The volume of gas-filled void space is then calculated as ($V_g \cong V_{VS} - M_{H_2O}$). Finally, the cell is placed in the water bath and evacuated close to the theoretical equilibrium vapor pressure of water at 25 °C (3.2 kPa). Pressure readings are logged at 1 min intervals over several weeks, and at least one reevacuation of the cell is conducted to allow determination of the rate constant governing hydrogen entry into the iron as described in the Calculation Methods section.

Calculation Methods

Apparent Corrosion Rate. The apparent corrosion rate for an iron sample is calculated from the increase in the cell's hydrogen content, as inferred from pressure measurements of the cell's void space over time (*17*). An example plot of the logged pressures versus time is presented in Figure 1a.

Two pressure reductions were carried out during this run, at 480 and 630 h. For the apparent rate calculation, the produced hydrogen is assumed to accumulate only in the liquid and gas phases.

$$\text{total moles } H_2 = \text{moles } H_{2\ aq} + \text{moles } H_{2\ gas}$$

Up until the first pressure reduction, P_{H_2} in the cell at each point in time is calculated as the difference between the total pressure (P_{tot}) and the initial pressure (P_{init}), which is a combination of contributions from the vapor pressure of water in the cell and the residual nitrogen gas present.

$$P_{H_2} = P_{tot} - P_{init}$$

From the ideal gas law, the moles of H_2 present in the gas phase are calculated

$$\text{moles } H_{2gas} = P_{H_2} V_g/(RT) \quad (3)$$

where R is the gas constant and T is in Kelvin. The moles of H_2 in the aqueous phase (normally < 10% of the total hydrogen in the cell) are calculated through Henry's law constant

$$\text{moles } H_{2(aq)} = K_H P_{H_2} M_{H_2O} \quad (4)$$

where M_{H_2O} is the mass of water in kilograms. At 25 °C, the Henry's law constant (K_H), calculated from the solubility of hydrogen in water (*18*), is equal to $10^{-5.124}$ for hydrogen pressures expressed in kPa. Finally, R_{app}, the apparent corrosion rate in mmol kg^{-1} d^{-1} is calculated as

$$R_{app} = 10^3\ [\text{moles } H_{2(aq+gas)} \text{ at } t_2 - \text{moles } H_{2(aq+gas)} \text{ at } t_1]/[M_{Fe}\ (t_2 - t_1)] \quad (5)$$

Substituting eqs 3 and 4 in 5 yields

$$R_{app} = 10^3 \left[\frac{V_g}{RT}(P_{H_2(t2)} - P_{H_2(t1)}) + K_H M_{H_2O}(P_{H_2(t2)} - P_{H_2(t1)})\right]/[M_{Fe}(t_2 - t_1)] \quad (6)$$

where M_{Fe} is the mass of iron in kilograms and t is in days. A plot of the apparent rates as calculated from eq 6 for the ISPAT iron is presented in Figure 1b.

Corrected Corrosion Rate. To determine the *corrected* or *actual* corrosion rate for an iron sample, the *apparent* rate must be corrected for the amount of hydrogen gas that directly enters the solid phase. This is a commonly recognized phenomenon that depends on many factors, including the structure, thermal-mechanical history, and composition of the iron material as well as the water composition, pressure, and temperature (*10*). Under anaerobic corrosion, atomic hydrogen is produced at the corroding surface. Some of this atomic hydrogen enters the iron lattice, and the balance undergoes recombination to molecular hydrogen gas. Certain elements form surface species that can either impede this recombination and thus promote hydrogen entry into the iron, such as P, As, Sb, Bi, S, and CN, or facilitate the recombination and thus inhibit hydrogen entry, such as Cd, Au, Ag, Pt, Cu, and Al (*19*, *20*). The rate of hydrogen entry is found to be dependent on the square root of the local partial pressure of hydrogen gas (*21*), which reflects dissociation of molecular hydrogen into individual atoms (adatoms) at the iron surface. The equilibrium solubility of hydrogen in iron and other metal lattices also varies with $P_{H_2}^{0.5}$, a relationship known as Sievert's law (*22*). Because of this same functional relationship for solubility and kinetic control, a subscript 'S' is associated with the reaction rate constant

$$R_{entry} = k_S P_{H_2}^{0.5} \quad (7)$$

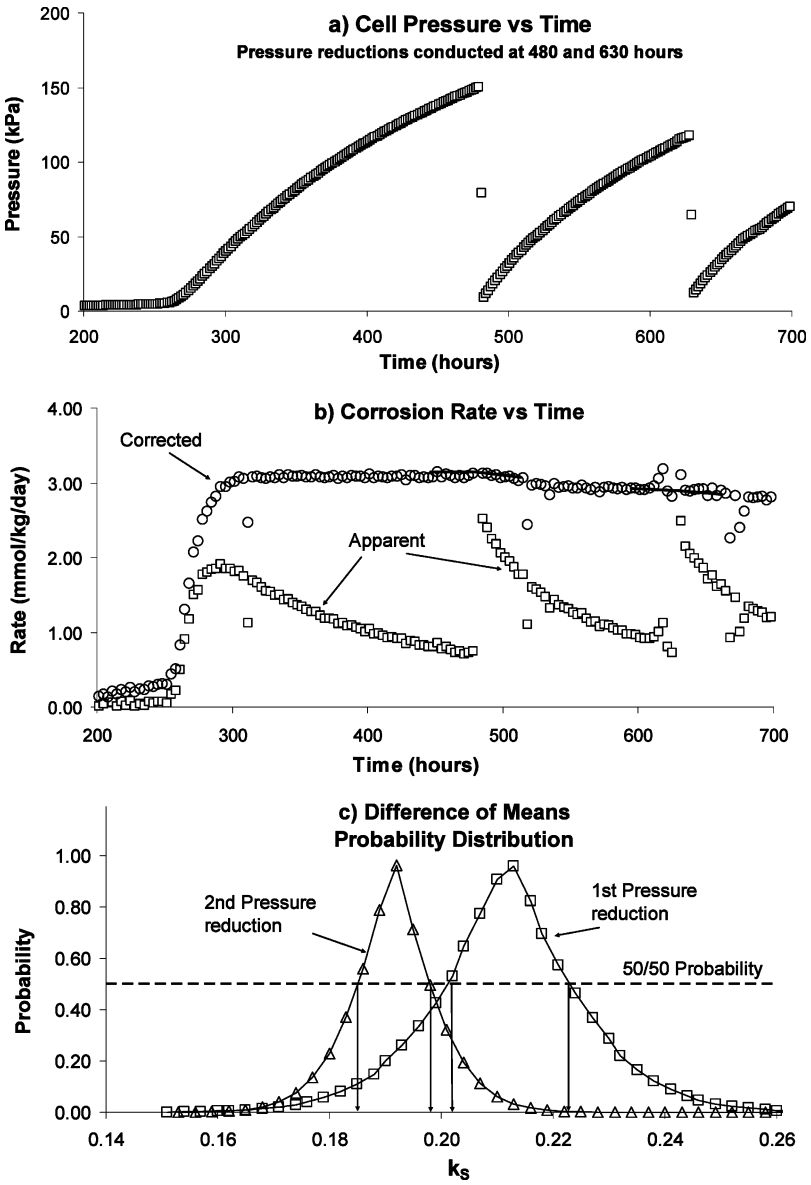

FIGURE 1. (a) *P* versus *t* for test cell containing ISPAT iron. Run conditions are recorded in Table 1. Note two pressure reduction steps at 480 and 630 h. (b) Apparent (squares) and overall (circles) rates of hydrogen production calculated from the cell pressure data in Figure 1a. Four regression lines, two on each side of the two depressurization times were used to estimate k_S values of 0.192 and 0.201 mmol kg^{-1} d^{-1} kPa$^{-0.5}$ at 480 and 630 h, respectively. (c) Probability distributions corresponding to the two depressurization events that indicate for a given k_S value the likelihood the means of R_{corr} values on each side of the depressurization time are equal.

where k_S has units of mmol kg^{-1} d^{-1} kPa$^{-0.5}$. The apparent corrosion rate (eq 6) can be adjusted for the amount of hydrogen entering the iron to yield an overall or corrected rate of corrosion

$$R_{corr} = \left[10^3 \left[\frac{V_g}{RT}(P_{H_2(t2)} - P_{H_2(t1)}) + K_H M_{H_2O}(P_{H_2(t2)} - P_{H_2(t1)})\right]/[M_{Fe}(t_2 - t_1)]\right] + k_S \bar{P}_{H_2}^{0.5} \quad (8)$$

where $\bar{P}_{H_2}$ is the average pressure over the time interval of the rate calculation. The value of the rate constant for an iron is determined by reducing the pressure in the cell at least once during the corrosion test. As shown for the ISPAT iron run in Figure 1b where pressure was reduced on two occasions, the apparent rate (open squares) immediately increases, producing sharp discontinuities. To determine the actual corrosion rates, the value of k_S is adjusted in the overall rate expression until the discontinuities in the data set are removed. The k_S that removes the discontinuity is determined computationally by increasing the value of k_S in 1% increments and calculating 20 corrosion rates over a 20−50 h interval, both before and after the discontinuity. A small amount of hydrogen degasses from the water phase immediately following the pressure reduction. This process is complete within 2 h of the pressure reduction (*17*), and so data for this period are omitted from the calculation procedure. Each set of data is then fit by simple linear regression using the FORTRAN subroutine FIT (*23*), to an equation of the following form: $R_{corr} = a + bt$. Both equations are solved to yield independent values for R_{corr} at the time of the pressure reduction. The selected k_S is the one that minimizes the difference between these two values. This procedure yields k_S values for the ISPAT iron of 0.201 and 0.192 for the first and second pressure reduction steps, respectively. A close scrutiny of Figure 1b reveals the pair of regression lines that were used to determine these k_S values. The corrected corrosion rates (open circles in Figure 1b) were calculated using an average k_S value of 0.197.

TABLE 2. Conductivity and pH Values of 1:1 Water/Fe Mixtures Equilibrated on a Rotary Mixer at Room Temperature for 1 h[a]

UW no.	name	pH	conductivity (μS/cm)
NA	Master Builders (+18 mesh)	8.91	18.9
114	Master Builders	11.33	534
12	Master Builders	11.21	330
NA	Master Builders (−80 mesh)	7.54	71.2
143	Connelly	7.47	145
223	Connelly	7.12	71.9
192	Connelly	6.70	163
147	Peerless	9.56	32.3
NA	Fisher Electrolytic	10.53	120
120	Gotthart-Maier	9.60	24.8
165	Gotthart-Maier	9.15	19.7
274	QMP	8.05	16.6
275	ISPAT	11.14	615
NA	Kanmet	7.77	850
121	Cercona	8.58	14.1

[a] NA-not available or not applicable.

As for the uncertainty in the derived k_S value, it is estimated by performing a Student's *t*-test on the means of 10 corrosion rates calculated over a 5 h interval on both sides of the discontinuity, again excluding data 2 h immediately after the pressure reduction. This procedure is performed for a range of k_S values that bracket the value obtained with the regression procedure. A plot of the Student's *t*-probability distributions corresponding to the two discontinuities obtained for the ISPAT iron are shown in Figure 1c. The 50% probability line demarcates a reasonable uncertainty in k_S. For example, between 0.202 and 0.223 for the first pressure reduction, the means of k_S on both sides of the pressure reduction are likely the same value. In other words, no discontinuity exists. Outside this range, a discontinuity likely still exists.

An alternate method to determine k_S is to choose the value that corresponds to the maximum in the probability distribution curve. For the ISPAT iron (Figure 1c), this approach yields values of 0.213 and 0.192 compared to 0.201 and 0.192 obtained by the regression technique for the two pressure reduction events. However, the regression technique is preferred because (1) it considers more data on each side of the discontinuity, (2) it does not require a zero slope in the corrected rate data as does constructing the probability distribution curve, and (3) although the probability distribution curves for the ISPAT iron in Figure 1c are symmetrical, asymmetrical and highly skewed distributions were obtained for other irons examined in this study, making it difficult to determine a representative uncertainty in k_S, let alone the value itself.

Results

The pH and conductance measurements on 1:1 water/ZVI extracts are recorded in Table 2.

Both show large variation, with conductance ranging from 14 to 850 μS cm^{-1} and pH from 6.7 to 11.3. It is noteworthy that water extracts of irons free from soluble constituents (i.e. lowest conductance) exhibit pH's closest to the theoretical equilibrium pH of 9.24, predicted for an iron/distilled water system under anaerobic conditions at saturation with respect to $Fe(OH)_2$ (*17*).

Since investigations into the mechanisms of dehalogenation by various sources of ZVI began in the early 1990s, the four most studied materials have been Master Builders, Connelly, Peerless, and Fisher Electrolytic. Corrosion test results for these materials are presented in Figures 2 and 3.

Two sets of data are shown for each iron: a lower set (open squares) represents the apparent corrosion rate, and an upper set (filled squares) represents the overall or corrected rate. The discontinuity in the trend of the apparent rate data serves as a basis to make this correction as described in the Calculation Methods section. The corrected corrosion rates for the three coarse-grained, prominently oxidized irons, Master Builders, Connelly and Peerless, are similar, within a factor of 3. In contrast, the corrosion rate for the fine, minimally oxidized, Fisher electrolytic iron in Figure 3 steeply rises, attains rates which are a factor of 200 times any of the other three irons, and then sharply drops, presumably as a result of the buildup of corrosion products, such as ferrous hydroxide precipitates. An integration of the area under the corrosion rate curve up to 200 h, at which time the rate had subsided, indicates that approximately 5% of the original sample had undergone corrosion.

Corrosion tests on different batches of the same iron usually yield similar results. Corrected rates for two batches

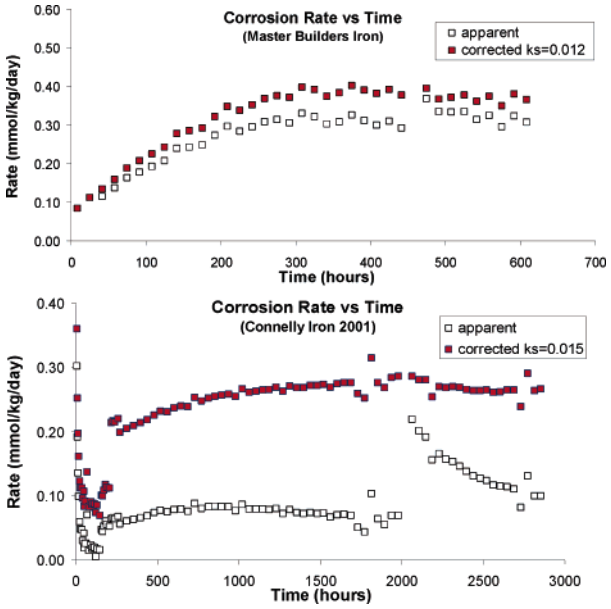

FIGURE 2. Apparent and corrected corrosion rates for Master Builders and Connelly irons.

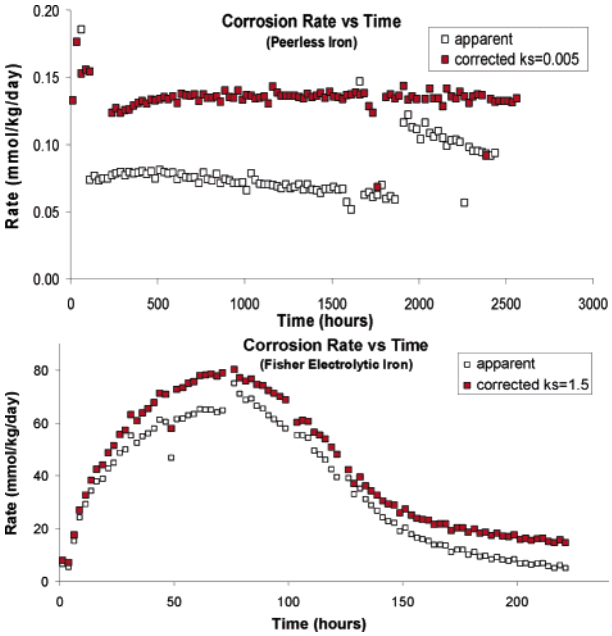

FIGURE 3. Apparent and corrected corrosion rates for Peerless and Fisher Electrolytic irons.

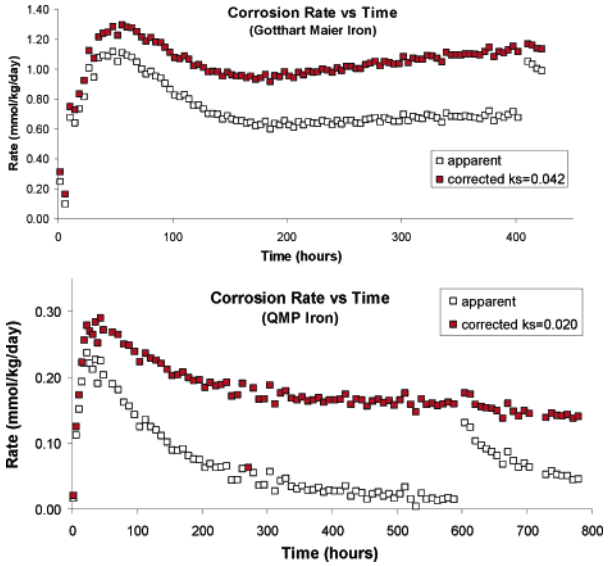

FIGURE 4. Apparent and corrected corrosion rates for Gotthart-Maier and QMP.

of Connelly iron carried out 3 years apart are presented as Supporting Information to this paper.

Corrosion rates were measured for three additional ZVIs: Gotthart-Maier, QMP, and ISPAT. Results for the first two are presented in Figure 4, and the ISPAT results were presented in Figure 1. ISPAT iron shows the most striking difference between the apparent and the corrected corrosion rate. It also took 250 h for hydrogen production to be measurable. After the apparent rate reached a maximum of 2 mmol kg^{-1} d^{-1}, there was a pronounced decrease. The 250 h delay in the onset of hydrogen is likely due to corrosion inhibition contributed by lime coatings on the particles. ISPAT iron is produced by the *sponge iron process*, which involves gas reduction of iron oxides at high temperatures. A lime injection/coating process is implemented to decrease particle clustering due to softening at the high kiln temperatures (*24*).

Discussion

With the exception of Gotthart-Maier, the other iron materials can be classified into two styles of corrosion behavior. The first style, exhibited by Fisher, QMP, ISPAT, and Master Builders, is characterized by a low initial corrosion rate, followed by a period of either sharp or gradual increase. After reaching a maximum, the rate slowly decreases. The QMP iron (Figure 4) amply reflects this behavior. Some time is required for the material to fully wet up and establish cathodic and anodic sites for the generation of hydrogen, which first must diffuse through water films before entering the gas phase of the test cell. The time required to establish noticeable hydrogen production varies from minutes to hours depending on the iron, as does the time required to reach a maximum rate. The QMP and Fisher iron begin corroding immediately, and the rates peak at 23 and 70 h, respectively. Due to a finer grain size, the Fisher corrosion rates are higher than the QMP rates, and thus the precipitation of iron hydroxides on the particle surfaces of Fisher iron must be greater. This would explain the much steeper decrease with time in the corrosion rate of Fisher iron after the maximum is reached, as compared to QMP. Master Builders iron (Figure 2) shows a more gradual increase toward a maximum corrosion rate than either the Fisher or QMP irons, probably reflecting a greater thickness of iron oxides initially present on the iron particle surfaces than the other two irons. The maximum rate was attained only after 300 h of water contact.

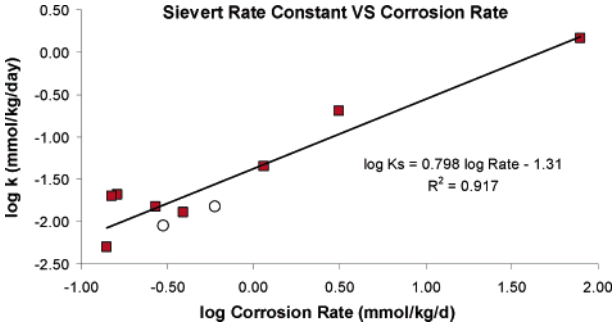

FIGURE 5. Correlation plot of the k_S vs R_{corr}. Squares refer to ZVI's samples listed in Table 1. Circles refer to measurements on a single sample of Master Builders iron over a 6-month period (*17*).

The second type of corrosion behavior is exhibited by the Connelly and Peerless irons. Both materials show high initial hydrogen production but decrease to a minimum around 200 h. A slow, progressive increase in rate then follows. Both irons were monitored for over 2500 h, and the rates ultimately level off. The Gotthart-Maier iron (Figure 4) emulates the corrosion behavior of the first group of irons, starting low, increasing to a maximum, and then slowly decreasing. However, after the maximum, the rate decreases to a minimum and begins to increase around 200 h. This peculiar behavior was traced to the presence of a small amount of Al metal particles in the iron. Al corrodes much faster under alkaline pH's than Fe, and the early maximum in the overall corrosion rate at around 50 h is likely due to the contribution of Al corrosion. If the Al effect were removed, Gotthart-Maier iron probably would behave similar to Master Builders.

Coarse grain size and thick oxide coatings (Master Builders) should contribute to a delay in hydrogen production, whereas fine grain size and thin oxide coatings (Fisher Electrolytic) should result in early hydrogen production. However, other factors may be involved, such as the composition of the iron and the water with which it is in contact. Although deionized water was used in all corrosion tests reported in this study, the iron material tested was 'as received'—not treated in any way to remove soluble salts or possible soluble acids and bases that may have been present. So the actual water composition developing in a corrosion test may differ from sample to sample. In the absence of any contribution of soluble material to the deionized water used in the corrosion test, chemical modeling shows that the pH of the water should rise to 9.24 and have a dissolved iron concentration of 0.6 mg/L (saturation with respect to $Fe(OH)_2$) (*17*). This should occur with a minimal amount of corrosion (0.011 mmol kg^{-1} L^{-1}). As an example calculation of the time required, consider the lowest corrosion rate material examined in this study: Peerless iron (0.14 mmol kg^{-1} d^{-1}). For a 1:1 mass ratio of iron to water, less than two hours is needed to attain saturation with respect to $Fe(OH)_2$. Assuming $Fe(OH)_2$ precipitation is unimpeded, subsequent corrosion should result in no further changes in the water composition.

Sievert Rate Constant. Important issues that relate to k_S include its variation with corrosion rate, time, and magnitude of the pressure reduction step undertaken to determine its value. An example to show the latter is unimportant is presented for the ISPAT iron in Figure 1. Two pressure releases are conducted: (1) from 150 to 8.9 kPa, a 141 kPa change and (2) from 117 to 12 kPa, a 105 kPa change. So despite a 25% difference in the pressure reduction, the derived k_S values are found to be within experimental uncertainty: 0.201 ± 0.011 and 0.192 ± 0.007, respectively. With respect to the variation of k_S with corrosion rate, Figure 5 shows a log−log plot for the various iron samples (see Table 1).

The R_{corr} values used correspond to the time each degassing step was conducted. The plot shows a significant positive correlation of k_S with R_{corr}. This was also observed in a 160 d test of Master Builders iron (*17*). In that study, k_S decreased by 40% as the corrosion rate decreased by 50% due to buildup of corrosion products. Both results show that a unique k_S cannot be ascribed to an iron material but is coupled to its corrosion rate at the time the k_S was measured. The positive correlation reflects the fact that hydrogen entry not only increases with the hydrogen pressure of the corrosion environment but also with the rate of production of hydrogen via the reaction of water molecules at the surface of the iron particles. For a single iron material, both k_S and R_{corr} ultimately will decrease over time with the accumulation of corrosion products.

The pathways by which hydrogen atoms can enter (and leave) the iron lattice are multiple, e.g. slowly through oxide films, more quickly at metal/water interfaces, or by direct production of hydrogen atoms through the corrosion of the iron surface by water molecules. Once having entered the iron lattice, hydrogen atoms may be associated with a variety of traps with different binding energies, such as lattice defects, voids, grain boundaries, microcracks, etc. Traps with low binding energies may be reversible, allowing hydrogen atoms to permeate and exit iron particles; whereas others may be permanent, allowing hydrogen to accumulate in the lattice. Hydrogen may also react with carbon molecules commonly present in the iron alloys that comprise commercial ZVI products. The reaction, called decarburization, produces methane gas that also accumulates in the iron lattice. Clearly, the adoption of a single rate constant to describe the complexity of hydrogen uptake dynamics in granular iron, as done in this study, is a simplistic approach, but one that potentially has practical application. An obvious improvement to the form of eq 7 is to recognize that there are at least two independent pathways by which H_2 gas can enter iron: (1) directly from the gas phase through sorption onto the iron surfaces, followed by dissociation into individual hydrogen atoms and migration into the lattice and (2) by failure of hydrogen atoms produced from corrosion at the solid/water interface to combine into hydrogen gas molecules where they otherwise would enter the water and gas phase. If these two entry processes work independently, it argues for the following relationship to correct the apparent corrosion rate for hydrogen entry into the iron lattice

$$R_{corr} = R_{app} + k_S P_{H_2}{}^{1/2} + \alpha R_{corr}$$

where α is the proportion of hydrogen produced by corrosion at the solid/water interface that ends up in entrapment sites in the iron lattice. Solving for R_{corr} yields

$$R_{corr} = \frac{R_{app} + k_S P_{H_2}{}^{1/2}}{1 - \alpha} \qquad (9)$$

Eq 9 is an improvement over eq 7 but increases the difficulty to design corrosion tests that allow derivation of two parameters rather than just one. Because of the current lack of such data, only the simpler one parameter relationship is invoked in the following modeling effort.

Controls on Hydrogen Pressure. The theoretical inorganic control on P_{H_2} at a PRB undergoing anaerobic corrosion is the equilibrium P_{H_2} for the overall iron corrosion reaction:

$$Fe_{(s)} + 2H_2O_{(l)} \leftrightarrow Fe(OH)_{2(s)} + H_{2(g)}$$

However, because $Fe(OH)_2$ is predicted to convert to magnetite (Fe_3O_4) via the Schikorr reaction (eq 2), the long-term control on P_{H_2} would presumably be imposed by the following reaction:

$$3Fe_{(s)} + 4H_2O_{(l)} \leftrightarrow Fe_3O_{4(s)} + 4H_{2(g)}$$

ΔG^o_f for all constituents except $Fe(OH)_2$ were taken from ref *25*. Data for $Fe(OH)_2$ were provided by Anderson (*26*). Calculated ΔG°_R values for the two reactions are −12.218 and −64.002 kJ. From the equilibrium constants for the above two reactions, determined using the expression $\Delta G^o_R = -RT\ln K$ at 25 °C, the following equilibrium P_{H_2} values are calculated

$$K_{Fe(OH)_2} = P_{H_2} = 10^{2.14} = 13\ 800\ \text{kPa}$$

and

$$K_{Fe_3O_4} = 10^{11.21} = P_{H_2}{}^4; \quad P_{H_2} = 10^{2.80} = 63\ 100\ \text{kPa}$$

Such high P_{H_2}'s may build up internally in iron materials that are undergoing anaerobic corrosion due to the migration of surface-sorbed H atoms into the iron lattice, where they may recombine into diatomic hydrogen gas at lattice defects, grain boundaries, or microcracks. The resulting high internal pressures account for the observed embrittlement and blistering of iron alloys and steels that are exposed to wet, anaerobic environments for long periods of time (*27*, *28*). In the porewater of granular ZVI/water systems, these high pressures are not attained. The reason is due to different dynamics for two processes: (1) the overall corrosion reaction, which produces hydrogen gas and (2) the entry of hydrogen into the iron phase. The first reaction normally attains a maximum rate in several hundred hours and then gradually decreases (R_{corr}), whereas the second reaction increases with the square root of the ambient hydrogen pressure ($R_{entry} = k_S P_{H_2}{}^{0.5}$). Thus in a closed system, as P_{H_2} increases, the proportion of produced hydrogen entering the iron phase increases relative to that entering the pore fluid and gas phase over time. At some P_{H_2} the two rates must become equal, i.e., the rate of hydrogen produced by corrosion equals the rate of hydrogen entering the iron.

$$R_{corr} = R_{entry} = k_S P_{H_2}{}^{0.5}$$

When this condition occurs, P_{H_2} in the pore network will have reached its maximum value, and the system will have attained a steady state. Consequently, anaerobic corrosion, as inferred from the production of hydrogen gas, will appear to have stopped. This maximum, or steady-state hydrogen pressure, can be calculated by rearranging the above relation:

$$P_{H_2SS} = \left[\frac{R_{corr}}{k_S}\right]^2 \qquad (10)$$

Over the long term, as corrosion products or precipitates accumulate on iron particle surfaces, this steady state or quasi-equilibrium P_{H_2SS} may change. Reardon (*17*) showed that over a 6-month corrosion test for Master Builders iron, R_{corr} and k_S decreased by similar amounts: 50% and 40%, respectively. These data are plotted in Figure 5 and follow the same relationship observed between k_S and R_{corrr} for all the ZVIs considered in this study. The similar decrease in the value of both parameters suggests that P_{H_2SS} as calculated from eq 10 may be relatively invariant with time. It is noted that in a closed system, P_{H_2} ultimately will attain P_{H_2SS}, but where there is groundwater flow to remove hydrogen in the dissolved state, the maximum attainable P_{H_2} may be less than P_{H_2SS}.

Predicting P_{H_2} Evolution at a Zerovalent Iron PRB. The change in P_{H_2} with travel distance through a PRB can be

calculated using a mixing cell approach. Assuming no bacterial utilization of the produced hydrogen, the hydrogen mass balance for the ith cell over time step Δt is then

$$H_{2(C)} - H_{2(S)} = H_{2(i+1)} - H_{2(i)} \quad (11)$$

where $H_{2(C)} - H_{2(S)}$ is the difference in the number of moles of hydrogen produced by corrosion and that having entering the iron lattice. $H_{2(i)}$ and $H_{2(i+1)}$ are the dissolved quantities of hydrogen entering and exiting the ith cell, respectively; i.e., the net hydrogen input into the groundwater over the interval, Δt. For cell length L (cm) and 1 cm^2 cross-sectional area, each cell contains $L\rho_{Fe}(1 - \Phi)/1000$ kg of ZVI (M_{Fe}) and $L\rho_{H_2O}\Phi/1000$ kg of groundwater (M_{H_2O}), where ρ_{H_2O} and ρ_{Fe} are the density of water and the particle density of iron, respectively; and Φ is the porosity. Making appropriate substitutions into eq 11 yields

$$R_{corr}\,\Delta t M_{Fe} - k_S \Delta t M_{Fe}[(P_i + P_{i+1})/2\,]^{0.5} + 10^3 M_{H_2O} K_H (P_i - P_{i+1}) = 0 \quad (12)$$

where Δt is given by L/v, and v is the average linear groundwater velocity. Equation 12 can be solved using the Newton−Raphson method for P_{i+1} (the hydrogen pressure of the groundwater leaving the ith cell). Example calculations using eq 12 for a 50 cm wall of Peerless and Connelly ZVI are included in the Supporting Information.

Pressures Higher than P_{H_2SS}. If pressures higher than P_{H_2SS} cannot develop in an iron/water system, what happens if hydrogen gas is added in excess of this limiting pressure? In this instance, R_{entry} would exceed R_{corr}, and the system hydrogen pressure should decrease until the steady-state pressure, P_{H_2SS}, is attained. In other words, an iron/water system can be designed, such that even though it is undergoing active anaerobic corrosion and hydrogen production, more hydrogen would be entering the iron than leaving. Thus, P_{H_2} of the porewater (and pore gas, if present) would decrease over time. The next phase of our research will examine the ability of the relations developed here to describe P_{H_2} decreases in hydrogen over-pressurized iron/water systems.

Acknowledgments

My appreciation to Randy Fagan for technical assistance and advice in conducting the corrosion tests, to Sean Andreao for performing the first batch of pH and conductivity measurements on iron/water extracts, and to Kathleen Waller, Andrzej Przepiora and Piotr Zarzycki for helpful suggestions and comments on the manuscript. I would also like to thank Marek Odziemkowski, Bob Gillham at Waterloo, and John Vogan and other researchers at EnviroMetal Technologies Inc. for their helpful discussions and continued interest and support of our iron corrosion research.

Supporting Information Available

A duplicate corrosion test on Connelly iron and on different mesh sizes of Master Builders, Fluka, and Peerless iron and P_{H_2} modeling incorporating groundwater flow with the use of eq 12 for Peerless and Connelly ZVI. This material is available free of charge via the Internet at http://pubs.acs.org.

Literature Cited

(1) Reynolds, G. W.; Hoff, J. T.; Gillham, R. W. Sampling bias caused by materials used to monitor halocarbons in groundwater. *Environ. Sci. Technol.* **1990**, *24*, 135−142.
(2) Senzaki, T. Removal of chlorinated organic compounds from wastewater by reduction process. III. Treatment of trichloroethylene with iron powder. *Kogyo Yosui* **1991**, *391*, 29−35.
(3) Gillham, R. W.; O'Hannesin, S. F. Metal-catalysed abiotic degradation of halogenated organic compounds. Modern Trends in Hydrogeology, International Association of Hydrogeologists. 1992, IAH Conference, 'Modern Trends in Hydrogeology', Hamilton, Ontario, Canada, 94-103.
(4) Gillham, R. W.; O'Hannesin, S. F. Enhanced degradation of halogenated aliphatics by zero-valent iron. *Ground Water* **1994**, *32*, 958−967.
(5) Matheson, L. J.; Tratnyek, P. G. Reductive dehalogenation of chlorinated methanes by iron metal. *Environ. Sci. Technol.* **1994**, *28*, 2045−2053.
(6) Gaspar, D. J.; Lea, A. S.; Engelhard, M. H.; Baer, D. R.; Miehr, R.; Tratnyek, P. G. Evidence for localization of reaction upon reduction of CCl_4 by granular iron. *Langmuir* **2002**, *18*, 7688−7693.
(7) Odziemkowski, M. S.; Simpraga, R. P. Distribution of oxides on iron materials used for remediation of organic groundwater contaminants − Implications for hydrogen evolution reactions. *Can. J. Chem.* **2004**, *82*, 1495−1506.
(8) Bonin, P. M. L.; Odziemkowski, M. S.; Gillham, R. W. Influence of chlorinated solvents on polarization and corrosion behaviour of iron in borate buffer. *Corros. Sci.* **1998**, *40*, 1391−1409.
(9) Ritter, K.; Simpraga, R. P.; Odziemkowski, M.; Irish, D. E.; Gillham, R. W. An In situ study of the effect of nitrate on the reduction of trichloroethylene (TCE) by granular iron. *J. Contam. Hydrol.* **2003**, *65*, 121−136.
(10) Zakroczymski, T. Entry of hydrogen into iron alloys from the liquid phase. In *Hydrogen Degradation of Ferrous Alloys*; Oriana, R. A., Hirth, J. P., Smialowski, M., Eds.; Noyes Publications: Park Ridge, NJ, 1985; Chapter 8, 888pp.
(11) Schikorr, G. Z. Uber die Reaktionen zwischen Eisen, seinen Hydroxyden und Wasser. *Elektrochim.* **1929**, *35*, 62−65.
(12) Shipko F. J.; Douglas D. I. Stability of ferrous hydroxide precipitates. *J. Phys. Chem.* **1956**, *60*, 1519−1523.
(13) Odziemkowski, M. S.; Schuhmacher, T. T.; Gillham, R. W.; Reardon, E. J. Mechanism of oxide film formation on iron in simulating groundwater solutions: Raman spectral and electrochemical studies. *J. Corros. Sci.* **1998**, *40*, 371−389.
(14) Cummings, J. Federal roundtable proposes national action plan for DNAPL source reduction. *Ground Water Curr.* **2000**, *35*, 4pp.
(15) Wilkin, R. T.; Puls, R. W. *Capstone Report on the Application, Monitoring, and Performance of Permeable Reactive Barriers for Ground Water Remediation*; EPA Report EPA/600/R-03/045a; 2003; Vol 1.
(16) Roggy, D. K.; Novak, P. J.; Hozalski, R. M.; Clapp, L. W.; Semmens, M. J. Membrane gas transfer for groundwater remediation: Chemical and biological fouling. *Environ. Eng. Sci.* **2002**, *19*, 563−575.
(17) Reardon, E. J. Anaerobic corrosion of granular iron: Measurement and interpretation of hydrogen evolution rates. *Environ. Sci. Technol.* **1995**, *29*, 2936−2945.
(18) Dean, J. A. *Lange's Handbook of Chemistry*, 14th ed.; McGraw-Hill Inc.: New York, 1992.
(19) Iyer, R. N.; Pickering, H. W. Mechanism and Kinetics of Electrochemical Hydrogen Entry and Degradation of Metallic Systems. *Annu. Rev. Mater. Sci.* **1990**, *20*, 299−338.
(20) Riecke, E.; Johnen, B.; Grabke, H. J. Effects of Alloying Elements on Corrosion and Hydrogen Uptake of Iron in Sulfuric Acid − Part III: Kinetics of Proton Discharge and Hydrogen Uptake at Binary Iron Alloys. *Mater. Corros.* **2004**, *36*, 455.
(21) Porter, A. S. Thompkins, F. C. The Kinetics of Chemisorption of Hydrogen and Carbon Monoxide on Evaporated Iron Films. *Proc. R. Soc. London, Ser. A* **1953**, *217*, 529−544.
(22) Sieverts, A.; Danz, W. Solubility of D_2 and H_2 in Palladium. *Z. Physik. Chem.* **1936**, *34(B)*, 158.
(23) Press, W. H.; Teukolsky, S. A.; Vetterling, W. T.; Flannery, B. P. *Numerical Recipes in FORTRAN*, 2nd ed.; Cambridge University Press: 1992; 964 pp.
(24) http://www.mty.itesm.mx/decic/centros/innova/climgateway/climateenglish/acindar00.htm.
(25) Robie, R. A.; Hemmingway, B. S.; Fisher, J. R. *Thermodynamic Properties of Minerals and Related Substances at 298.15 K and 1 Bar Pressure and at Higher Temperatures*; U.S. Geological Survey Bulletin 1452; U.S. Gov't Printing Office: Washington, DC, 1979; 456 pp.
(26) Anderson, G. M. *Thermodynamics of Natural Systems*, 2nd ed.; Cambridge University Press: 2005; 655 pp.
(27) Oriani, R. A. Hydrogen embrittlement of steels. *Annu. Rev. Mater. Sci.* **1978**, *8*, 327−357.
(28) Dayal, R K.; Parvathavarthini, N. Hydrogen embrittlement in power plant steels. *SADHANA* **2003**, *28*, 431−451.

Received for review March 15, 2005. Revised manuscript received June 23, 2005. Accepted June 26, 2005.

ES050507F